Optoelectronic Properties of KDP by First Principle Calculations

ARTICLE *in* INTERNATIONAL JOURNAL OF QUANTUM CHEMISTRY · MARCH 2013

Impact Factor: 1.43 · DOI: 10.1002/qua.24258

3 AUTHORS, INCLUDING:

H. A. Rahnamaye Aliabad
Hakim Sabzevari University
51 PUBLICATIONS **166** CITATIONS
SEE PROFILE

Iftikhar Ahmad
University of Malakand
106 PUBLICATIONS **629** CITATIONS
SEE PROFILE

Optoelectronic Properties of KDP by First Principle Calculations

Hossein Asghar Rahnamaye Aliabad,*[a] Marjan Fathabadi,[a] and Iftikhar Ahmad[b]

The optoelectronic properties of KDP (KH_2PO_4), in orthorhombic and tetragonal phases, have been investigated by generalized gradient approximation (GGA) and mBJ-GGA within density functional theory. The calculated fundamental indirect band gaps for orthorhombic and tetragonal KDPs are 2.83 and 4.35 eV, respectively. The calculated effective mass of electron, in this compound, is very close to the effective mass of carriers in a bilayer graphene. The electron density plots show that the covalent bonds between P and O within the PO_4 tetrahedra are symmetric in tetragonal phase, whereas in the orthorhombic phase this symmetry breaks, which affects the covalent bonds among the tetrahedra. The comparison of the calculated optical spectra by GGA and mBJ-GGA with the experimental results reveals that the optical dispersion spectra by mBJ-GGA are in closer agreement with the experimental results. © 2012 Wiley Periodicals, Inc.

DOI: 10.1002/qua.24258

Introduction

The potassium dihydrogen phosphate, KH_2PO_4 (KDP), crystal has many applications in optical devices such as electro-optical polarizers and modulators in laser systems and is also used as an efficient harmonic generator with high damage threshold. It is used for second and third harmonic generation in Nd:YAG lasers. Other important electro-optical materials similar to KDPs are ammonium dihydrogen phosphate (ADP), DKDP, and DADP crystals.[1] Experimental results show that KDP is transparent below 0.18 μm.[2] There is a good relationship between the crystal structure and optical response of materials. The linear and second-order nonlinear optic (NLO) properties of any crystal can be determined properties of all constituent chemical bonds. In KDP and ADP crystals, hydrogen bonds play an important role in the molecular structure, which strongly affect NLO responses of both crystals.[3]

The KDP crystal has ferroelectric and paraelectric properties, phase transition at low and high temperatures.[4,5] The phase transition from paraelectric to ferroelectric is reported at 123 K. A decrease in temperature changes the crystal symmetry from tetragonal (with I42d space group) in the paraelectric phase to orthorhombic (with Fdd2 space group) in the ferroelectric phase. In KDP crystal, the substitution of deuterium for hydrogen enormously affects this transition temperature. The transition of phases has been investigated experimentally and theoretically by different research groups.[6,7] It has also been reported that at 453 K the phase of the KDP crystal changes from tetragonal to monoclinic.[8,9]

Shenoy et al.[10] have investigated the formation of mixed crystals of pure ADP, KDP, and mixed crystals of $K_{1-x}(NH_4)_xH_2PO_4$ by slow evaporation from the supersaturated solution at an ambient temperature 27◦C. They observed that the thermal dehydration in ADP, KDP, and mixed crystals is associated with decomposition. Their results also show that an increase in NH_4 concentration decreases the decomposition temperature. Recently, Duchateau et al.[11] have reported the dynamics of electrons and holes in potassium dihydrogen phosphate (KH_2PO_4 or KDP) crystals. They observed two relaxation dynamics in KDP and DKDP crystals.

The extensive applications of KDP in optoelectronic make it an important optical material. Hence, in the present theoretical studies, attention has been paid to the optoelectronic properties of tetragonal and orthorhombic phases of KDP. The tetragonal and orthorhombic phases of KDP are shown in Figure 1. The lattice constants used in the present investigation are $a = b = 7.4529$ and $c = 6.971$ Å for tetragonal[12] and also $a = 10.546$, $b = 10.466$, and $c = 6.9261$ Å for orthorhombic crystal structures.[13]

Computational Details

The optoelectronic properties of these crystal structures are investigated by the highly accurate FP-LAPW method as implemented in the wien2k code.[14] Generalized gradient approximation (GGA) and modified Becke and Johnson GGA are used for the exchange-correlation interaction. The mBJ-GGA potential V_{xc}[15] uses mBJ exchange potential plus GGA correlation potential and performs the calculation of band gaps with accuracy similar to the computationally expensive GW calculations. This method provides gaps almost equal to the experimental values.

In solving the Kohn–Sham equations, the relativistic effects have been taken into consideration. In the calculations, the selected parameter that determines the size of the secular

[a] H. A. R. Aliabad, M. Fathabadi
Department of Physics, Hakim Sabzevari University, Sabzevar, Iran
[b] I. Ahmad
Department of Physics, University of Malakand, Chakdara, Pakistan
E-mail: rahnama@sttu.ac.ir or h_rahnamay@yahoo.com

matrix is RMT * $K_{max} = 4$, where the RMT is muffin-tin sphere radii and K_{max} is the cut-off wave vector in the first Brillion zone (B.Z). The selected muffin-tin radii for K, H, P, and O are 1.8, 0.84, 1.62, and 1.28 (in atomic unit) respectively. The iteration process was stopped after the calculated total energy was converged to less than 0.0001 Ry.

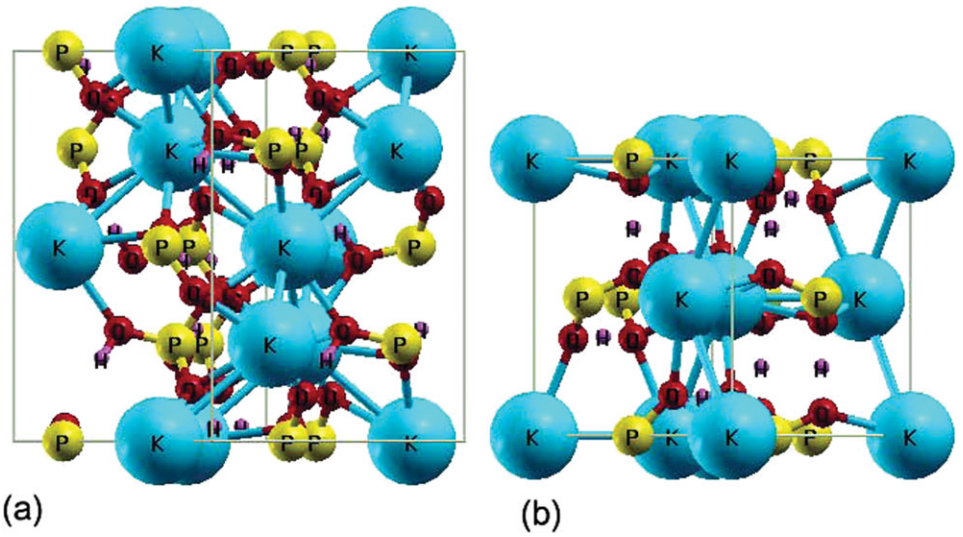

Figure 1. Unit cells of KDP in (a) orthorhombic and (b) tetragonal crystal structures. [Color figure can be viewed in the online issue, which is available at wileyonlinelibrary.com.]

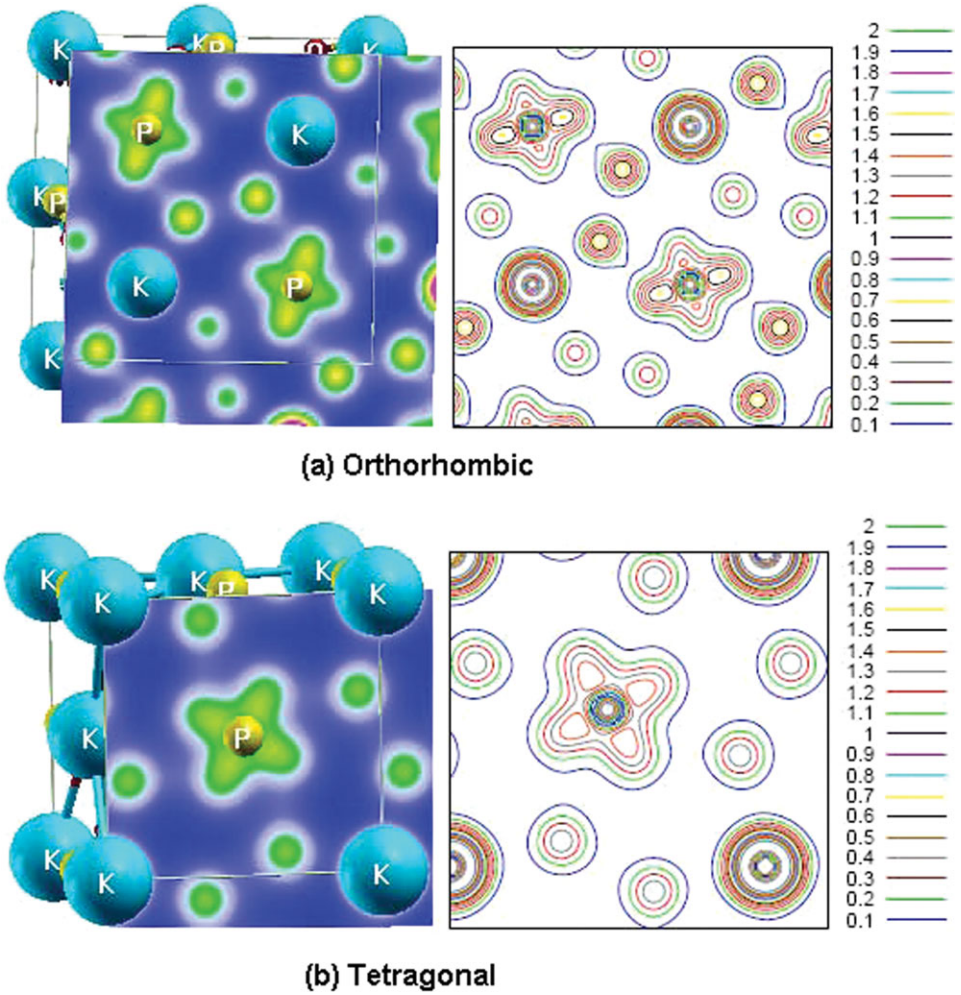

Figure 2. Electron density for KDP in (a) orthorhombic and (b) tetragonal crystal structure. [Color figure can be viewed in the online issue, which is available at wileyonlinelibrary.com.]

Result and Discussion

Electron density

In first principle calculations, the electron density plays an important role in the interpretation of the physical and chemical properties of a compound. Based on the electronic cloud, the bonding nature of KDP is presented in Figure 2 in [0 0 1] direction.

The results presented in the plots show strong covalent bonding within the PO_4 tetrahedra, in both phases. The electronic cloud for the tetragonal KDP reveals that the bonds within the PO_4 tetrahedra are symmetric, and the strength of each covalent bond is the same. Unlike the tetragonal KDP, the electronic clouds for the P—O bonds in the orthorhombic structure are not symmetric and have different covalencies. If we compare the results with the tetragonal structure, the covalency of the P—O bond is decreased, whereas it increases for those bonds in which O is away from H. This interesting behavior of covalency from tetragonal to orthorhombic structures within the PO_4 tetrahedra is also reported in Ref. [16]. The PO_4 networks are interconnected by chain of hydrogen O—H—O bonds, and these hydrogen bonds an ionic bonding between K and the PO_4 group also exists. Hydrogen bonds have important role for the stability of this structure, and the obtained results are in good agreement with experimental results.[17–19]

Band structure and band gaps

The band structures of the orthorhombic and tetragonal crystals of KDP are calculated along the high symmetry

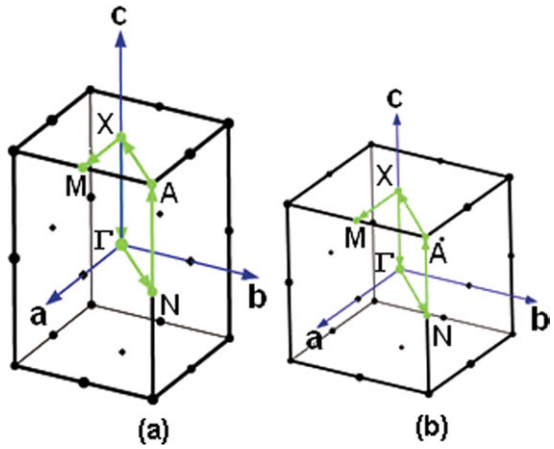

Figure 3. Selected directions in primitive Brillouin zone for KDP in a) orthorhombic and b) tetragonal crystal structures. [Color figure can be viewed in the online issue, which is available at wileyonlinelibrary.com.]

directions in the primitive Brillouin zone, shown in Figure 3. The calculated fundamental band gap for the orthorhombic crystal is 2.83 eV by GGA and 10.04 eV by mBJ-GGA, whereas for the tetragonal crystal it is 4.35 eV by GGA and 10.24 eV by mBJ-GGA.

The calculated band structures for both the phases of KDP are shown in Figure 4. The scale of energy in all figures is in eV, and the top of the valence band is set at zero (Fermi level) on the energy scale. It is clear from the results that the fundamental band gaps for both structures are indirect. The calculated results are compared with the experimental values in Table 1. The table reveals that the band gap of tetragonal is larger than orthorhombic. The table also shows that the calculated band gaps by GGA are smaller than the experimental results but are larger than the other first principle results. On the other hand, the obtained band gaps by mBJ-GGA are larger than the experimental values, whereas similar trend for the results of this approximation is also observed for other compounds.[15] This discrepancy in density functional theory (DFT) calculation mainly arises due to the approximations used for the exchange correlation. The diagonal elements of the effective mass tensor, m_e, for the electrons in the conduction band are calculated in $\Gamma \rightarrow$ N direction in k space using the following well-known relation:

$$\frac{1}{m_e(k)} = \frac{1}{\hbar^2}\frac{\partial^2 E(k)}{\partial k^2} \qquad (1)$$

The effective mass of electron is determined by fitting the electronic band structure to a parabolic function [Eq. (1)] in the first Brillouin zone using GGA and mBJ-GGA approaches. The effective mass of electron for the orthorhombic and tetragonal KDP are obtained from the curvature of the conduction band at Γ point.

The calculated electron effective mass for KDP in $\Gamma \rightarrow$ N direction are 0.024 m_e (orth. GGA), 0.039 m_e (orth. mBJ-GGA), 0.016 m_e (tetra. GGA), and 0.030 (tetra. mBJ-GGA). It is obvious that the calculated values by the mBJ-GGA are larger than the GGA values. The obtained results show that these values are closer to the effective mass of carriers in $B_{0.03}Ga_{0.91}In_{0.06}As$ (0.093 m_e[20]) and bilayer graphene (0.032 m_e[21]) compounds. The effective mass of electron in the conduction band for orthorhombic phase is larger than the tetragonal phase, so the mobility of electrons in the tetragonal phase is higher than the orthorhombic phase.

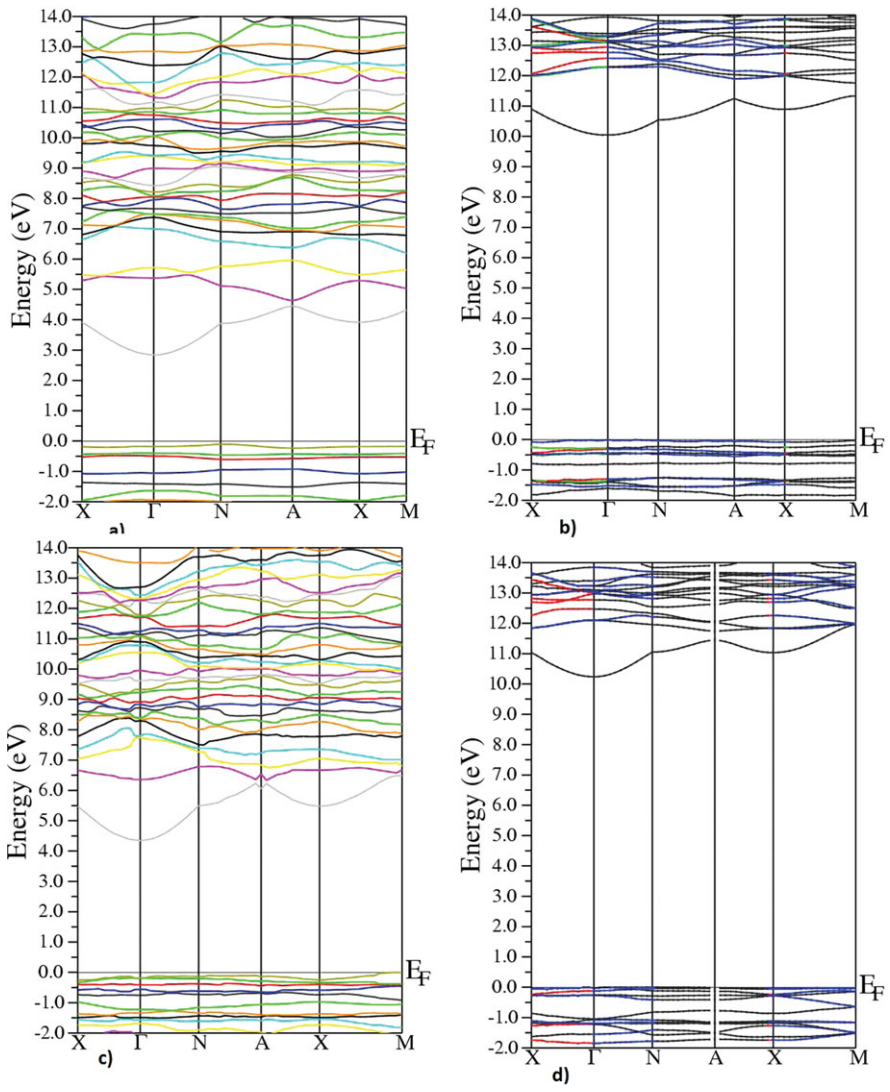

Figure 4. The calculated band structures for orthorhombic (a: GGA and b: mBJ-GGA) and tetragonal (c: GGA and d: mBJ-GGA) crystal structures. [Color figure can be viewed in the online issue, which is available at wileyonlinelibrary.com.]

Table 1. Calculated band gaps and effective mass of carriers for KDP.

	This work		Others	
Compounds	GGA	mBJ-GGA	Theory	Expt.
KDP (orth.)				
E_g (eV)	2.83	10.04	–	–
m^*/m_e ($\Gamma \rightarrow$ N)	0.024	0.039	–	–
KDP (tetra.)				
E_g (eV)	4.35	10.24	4.178[23]	7.12[24]
m^*/m_e ($\Gamma \rightarrow$ N)	0.016	0.030	–	–

Approximately, in all compounds, heavy carriers move with slower velocities, so the mobility of carriers is small. Typically materials made of elements with small electronegativity difference have high mobility and low effective mass, whereas materials with narrow bands (such as ionic compounds) have high effective mass and low mobility.[22]

Density of states

The electron distribution in an energy spectrum is described by the density of states (DOS), which can be measured experimentally in photoemission spectroscopes. The calculated total and partial DOS for KDP are shown in Figure 5. There are two nonequivalent positions for oxygen (O(I),O(II)) in orthorhombic phase.

The figure reveals that there are a large number of relatively localized states at the top of the valance band, originating mainly from the O-2p and P-3p with covalent admixtures between them. The lower conduction band consists of K/P-3p and O-2p states. The localized K-p state is located about −12.5 eV for orthorhombic and between −10 and −12.5 eV for tetragonal phase. Strong hybridization is observed between O and P orbitals.

Dielectric function

The transition between occupied and unoccupied states, including plasmons and single particle excitations, are caused by the electric field of a photon. A linear response of a material to an electromagnetic radiation is described by the dielectric function $\varepsilon(\omega)$, which can be obtained by the following well-known relation[25]:

$$\mathrm{Im}\varepsilon_{\alpha\beta}^{\{\mathrm{inter}\}}(\omega) = \frac{\hbar^2 e^2}{\pi m^2 \omega^2} \sum_{c,v} \int d\mathbf{k} \langle c_k|p^\alpha|v_k\rangle\langle v_k|p^\beta|c_k\rangle \times \delta(\varepsilon_{ck} - \varepsilon_{vk} - \omega) \quad (2)$$

The interband expressions in the corresponding real parts can be obtained by Kramers–Kronig transformation:

$$\mathrm{Re}_{\alpha\beta}^{\{\mathrm{inter}\}}(\omega) = \delta_{\alpha\beta} + \frac{2}{\pi} P \int_0^\infty \frac{\omega' \mathrm{Im}\varepsilon_{\alpha\beta}(\omega')}{(\omega')^2 - \omega^2} d\omega' \quad (3)$$

In the cubic crystal structure, the optical spectra are isotropic along the crystallographic *a*, *b*, and *c* axes. So, according to the symmetry of the crystal, the dielectric tensor has only one dependent component ($\varepsilon_{xx} = \varepsilon_{yy} = \varepsilon_{zz}$). The real parts of the frequency-dependent dielectric function for KDP are shown in Figures 6a–6d for *x*, *y*, and *z* components. The static dielectric permittivity tensor, $\varepsilon_1(0)$, of a nonpolar material contains electronic (high frequency) and ionic contribution. The high-frequency dielectric $\varepsilon_1(\infty)$ of the pure KDPs are presented in Table 2.

Refractive index is the square of dielectric constant. This compound is birefringent, because the obtained values are different for the *x*, *y*, and *z* directions. The obtained results by GGA are higher than the mBJ-GGA values. The calculated resonance energies ($\hbar\omega_0$) by GGA show three values in the *x*, *y* and *z* directions for the orthorhombic phase. It is also noted from the table that the obtained values by mBJ-GGA are larger than the GGA values. The imaginary parts of the frequency-dependent dielectric function for KDPs are presented in Figure 7 for *x*, *y*, and *z* components. The peaks on the Im $\varepsilon(\omega)$ curves for KDP (E_0, E_1, E_2, E_3, E_4) are related to the interband transitions from the valence to the conduction band states along N–Γ, N–X, N–A, and N–M directions. In comparison with the partial DOS (Fig. 5), the energy peaks on the Im $\varepsilon(\omega)$ by GGA from 2.83 to 12.83 eV and 4.35 to 14.35 eV are due to the electron transition between O-p (valence

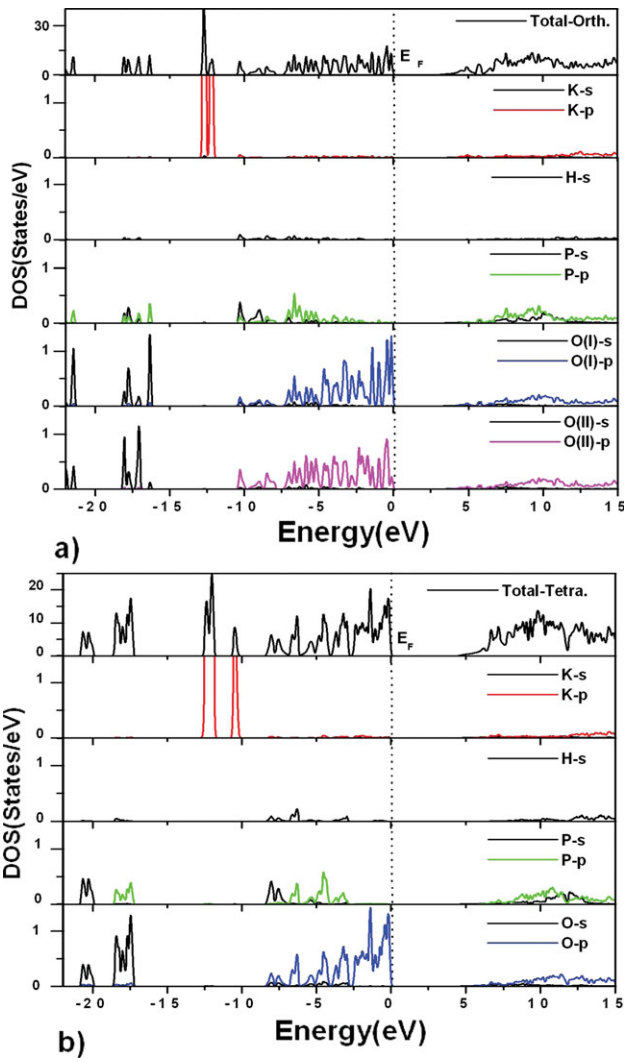

Figure 5. Total and partial DOS for a) orthorhombic and b) tetragonal crystal structures by GGA. [Color figure can be viewed in the online issue, which is available at wileyonlinelibrary.com.]

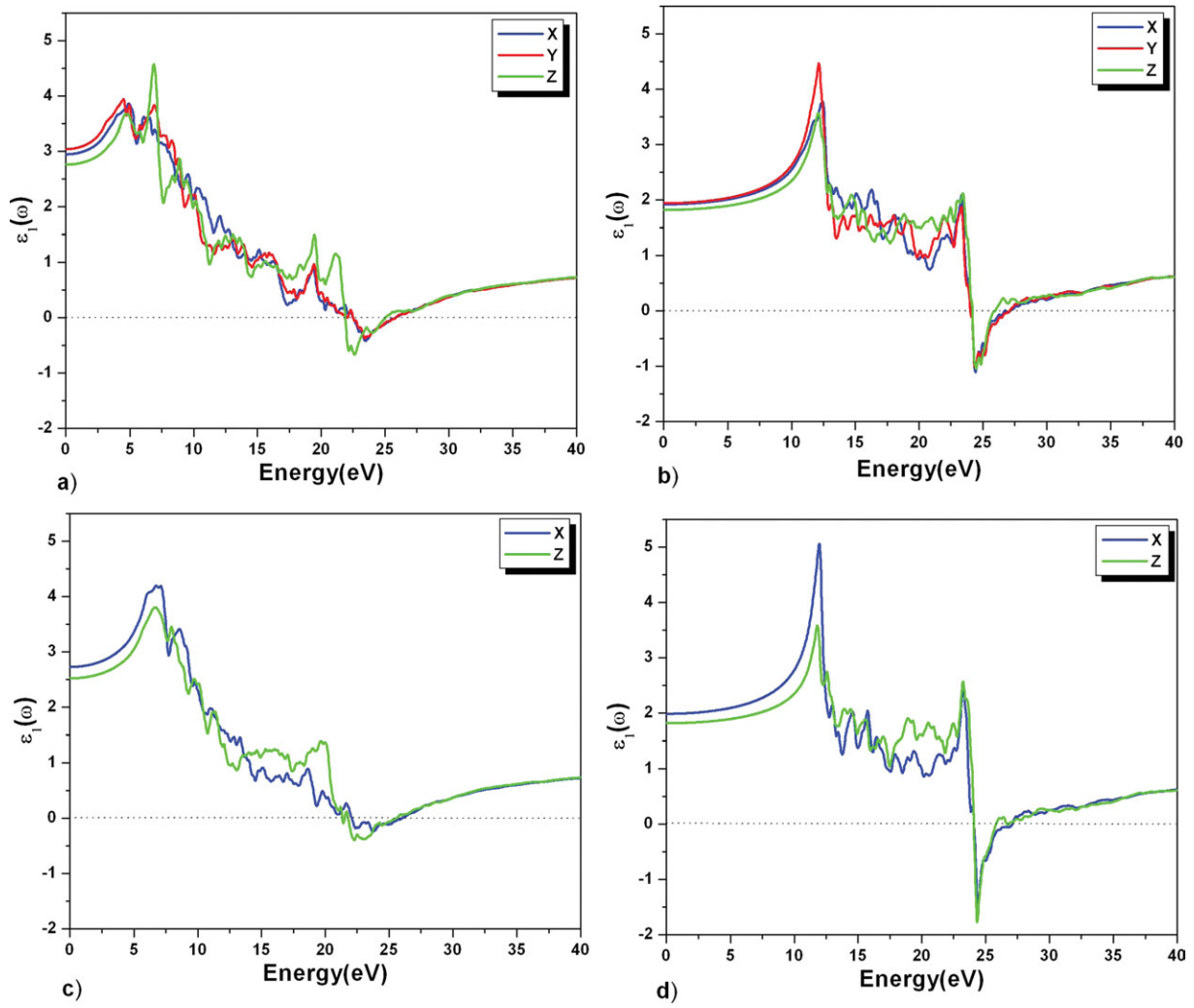

Figure 6. The real part of dielectric function for orthorhombic (a: GGA and b: mBJ-GGA) and tetragonal (c: GGA and d: mBJ-GGA) crystal structures. [Color figure can be viewed in the online issue, which is available at wileyonlinelibrary.com.]

band state) and P-p (conduction band state) for orthorhombic and tetragonal phases, respectively, whereas higher energy is related to K-p states. The fourth peak around 16–18 eV is related to the electron excitation from the O-2s state to the lower conduction band.

Electron energy loss spectroscopy

The electron energy loss spectroscopy (EELS) is a valuable tool for the investigation of various aspects of a material.[26] It plays important role in the design of dielectric materials, because it covers complete energy range including nonscattered and elastically scattered electrons (zero loss) as well as electrons that excite in an atom's outermost shell (valence loss) or valence interband transitions. The fast electrons excite the inner shell electrons (core loss) or induce core level excitation of near edge structure and XANES. In the case of interband transitions, this consists mostly of plasmon excitations. The scattering probability for volume losses is directly connected to the energy loss function. One can then calculate the EEL spectrum from the following relation[27]:

$$\text{EEL spectrum} = \text{Im}\left(\frac{-1}{\varepsilon_{\alpha\beta}(\omega)}\right) = \frac{\varepsilon_2}{\varepsilon_1^2 + \varepsilon_2^2} \quad (4)$$

In Figure 8, the energy loss function is plotted for the different phases of KDP for *x*, *y*, and *z* directions, in the energy range 0–40 eV. The figure has few main peaks, which can be related to single particle excitation, from the valence band (O-2s state) to the lower and upper conduction bands. The energy of the

Table 2. High-frequency dielectric constants $\varepsilon(\infty)$ and $\hbar\omega_0$ for KDP.

	GGA		mBJ-GGA	
Compounds	$\varepsilon(\infty)$	$\hbar\omega_0$ (eV)	$\varepsilon(\infty)$	$\hbar\omega_0$ (eV)
KDP (orth.)				
X	2.95	22.50	1.92	24.00
Y	3.04	22.00, 22.09, 22.50	1.94	24.00
Z	2.76	21.90	1.82	24.19
KDP (tetra.)				
X	2.73	22.06	1.99	24.08
Z	2.52	21.31, 21.50, 21.79	1.82	24.08

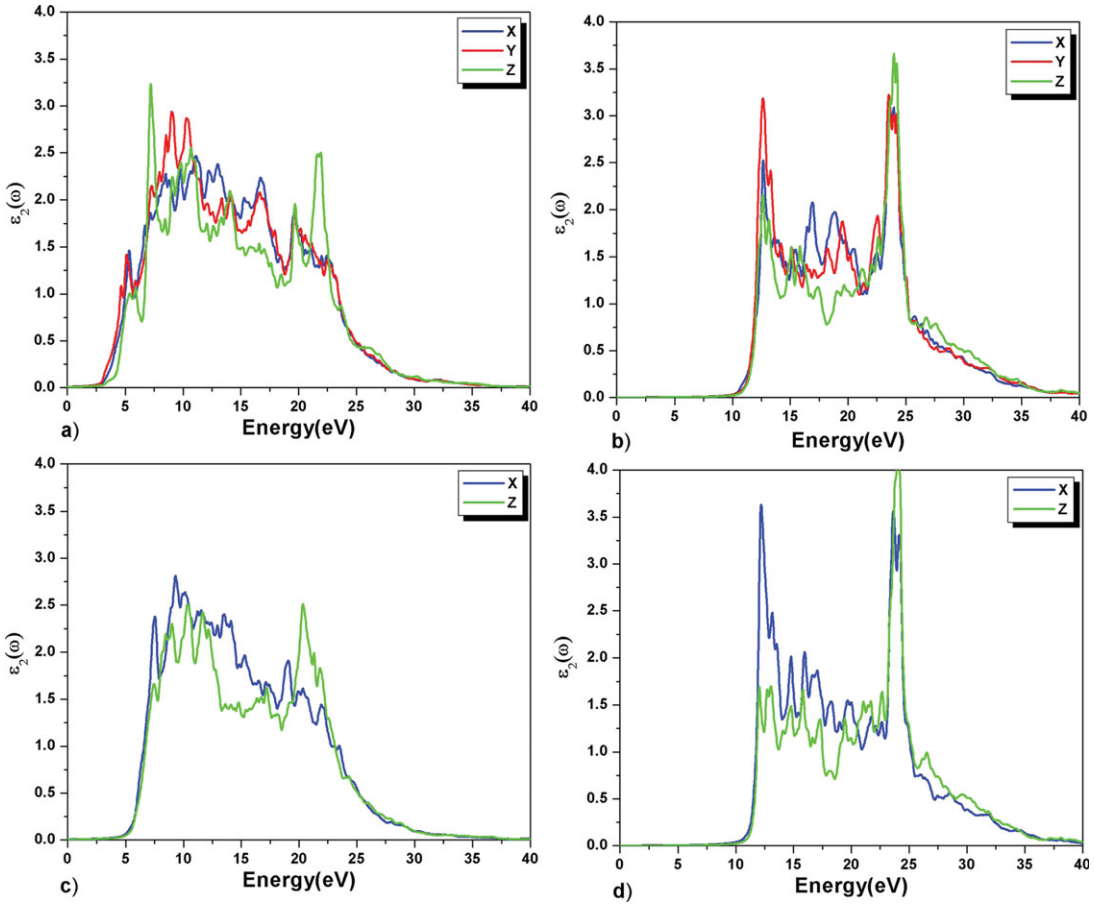

Figure 7. Imaginary part of dielectric function for orthorhombic (a: GGA and b: mBJ-GGA) and tetragonal (c: GGA and d: mBJ-GGA) crystal structures. [Color figure can be viewed in the online issue, which is available at wileyonlinelibrary.com.]

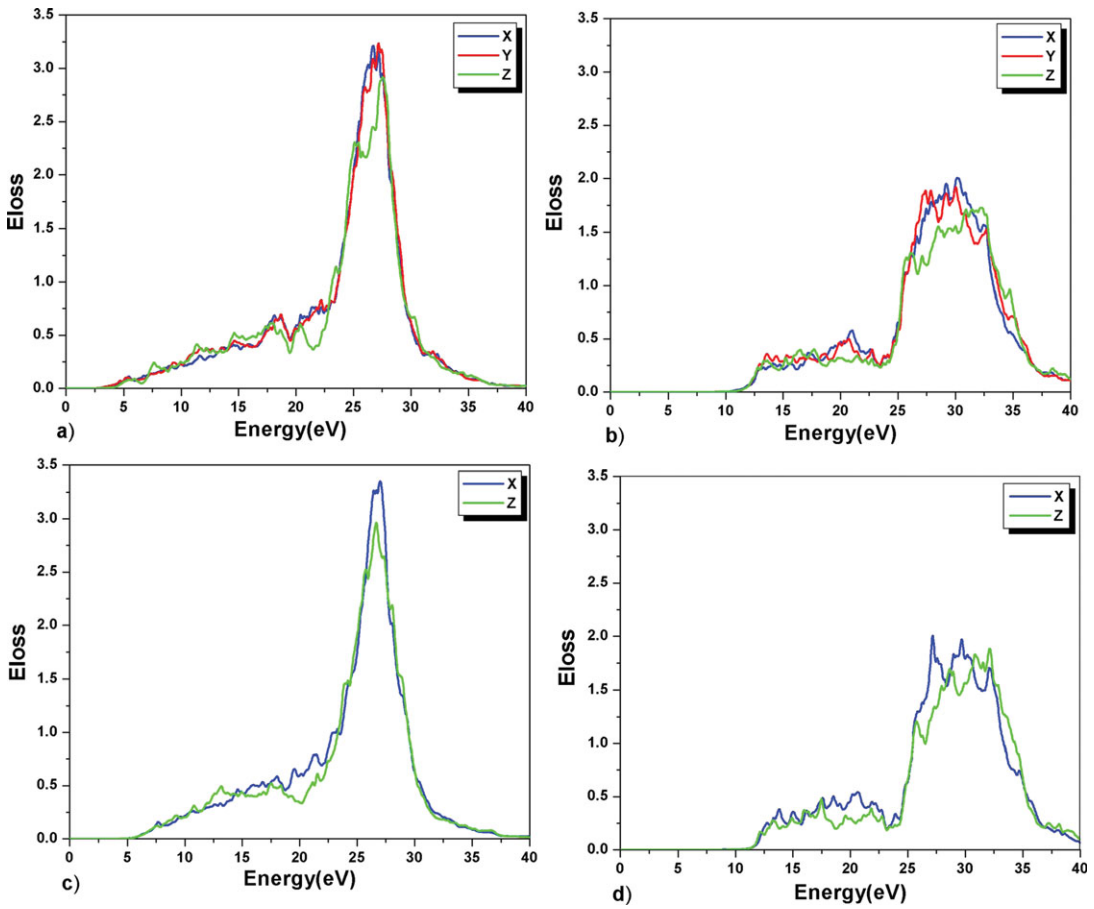

Figure 8. Electron energy loss for orthorhombic (a: GGA and b: mBJ-GGA) and tetragonal (c: GGA and d: mBJ-GGA) crystal structures. [Color figure can be viewed in the online issue, which is available at wileyonlinelibrary.com.]

Table 3. Calculated plasmon energy for KDP.

Compounds	$\hbar\omega_p$ (eV; GGA)	$\hbar\omega_p$ (eV; mBJ-GGA)
KDP (orth.)		
X	26.71	30.19
Y	27.17	30.01
Z	27.53	32.22
KDP (tetra.)		
X	27.01	27.17
Z	26.67	32.15

maximum of $\mathrm{Im}[-\varepsilon^{-1}(E)]$ can be related to the energy of volume plasmon ($\hbar\omega_p$). The values of $\hbar\omega_p$ obtained in this work are given in Table 3. It is observed from these results that mBJ-GGA method predicts higher plasmon energies as compared to GGA.

Refractive index and dispersion

For frequency doubling and for generation of sum and difference frequencies, it is required that the incoming and generated lights are in a defined phase relation along the path of interaction. It is well known to phase matching. Birefringent phase matching is a technique for achieving phase matching of a nonlinear process by exploiting the birefringence of a nonlinear crystal. Therefore, the birefringence properties of KDP as nonlinear crystal ($n_o > n_e$) make this compound potential candidate for these applications.[28] The calculated wavelength dispersions of refractive index for KDP crystals are shown in Figure 9. As a phase matching crystal, KDP has different refractive indices in the different directions (*x*, *y*, and *z*).

The curves are fairly flat in the long-wavelength region and decay rapidly for shorter wavelengths, showing a typical shape of the dispersion curve near an electronic interband transition. The calculated refractive indices for orthorhombic phase are higher than the tetragonal phase. The calculated results and experimentally measured values of the refractive indices at various wavelengths for tetragonal phase are summarized in Table 4. The table reveals that the results are underestimated by mBJ-GGA and overestimated by GGA. Furthermore, the mBJ-GGA results are closer to the experimental results than the GGA results.

Conclusions

The optoelectronic properties of KDP in orthorhombic and tetragonal phases are investigated using DFT with GGA and

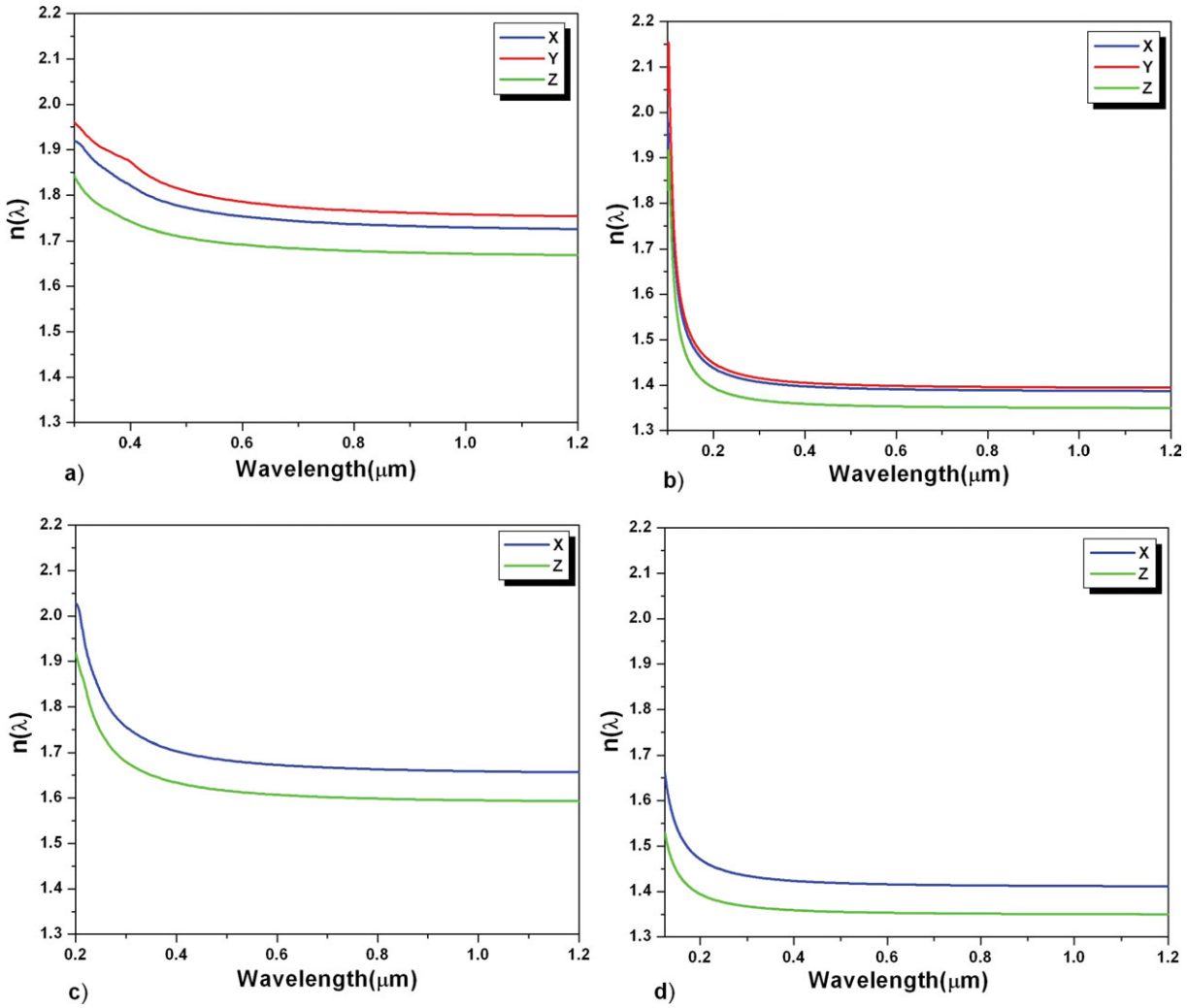

Figure 9. Refractive index (*n*) as function of wavelength for orthorhombic (a: GGA and b: mBJ-GGA) and tetragonal (c: GGA and d: mBJ-GGA) crystal structures. [Color figure can be viewed in the online issue, which is available at wileyonlinelibrary.com.]

International Journal of QUANTUM CHEMISTRY

Table 4. Refractive index (n) for selected wavelengths for KDP in tetragonal phase.

Wavelength (μm)	This work			Δn (this work)		Δn
	GGA	mBJ-GGA	Others	GGA	mBJ-GGA	Others
0.266						
n_o	1.7990	1.442	1.5590[a]	0.0819	0.070	0.0494
n_e	1.7171	1.372	1.5105[a]			
0.3547						
n_o	1.7198	1.427	1.5318[a]	0.0714	0.065	0.0454
n_e	1.6484	1.362	1.4864[a]			
0.532						
n_o	1.6789	1.417	1.5129[a]	0.0664	0.063	0.0420
n_e	1.6125	1.354	1.4709[a]			
0.5893						
n_o	1.6738	1.416	1.5098[a]	0.0659	0.063	0.0411
n_e	1.6070	1.353	1.4687[a]			
0.6328						
n_o	1.6703	1.415	1.5079[a]	0.0654	0.062	0.0406
n_e	1.6049	1.353	1.4673[a]			
0.6943						
n_o	1.6672	1.414	1.5055[a]	0.0651	0.061	0.0397
n_e	1.6021	1.353	1.4658[a]			
1.064						
n_o	1.6580	1.412	1.494[a], 1.495[b] 1.552[c]	0.0639	0.062	0.034, 0.035, 0.042
n_e	1.5941	1.350	1.460[a], 1.460[b] 1.510[c]			

[a] Expt.: Ref. [2]. [b] Expt.: Ref. [26]. [c] Theory (DFT): Ref. [23].

mBJ-GGA. The calculated fundamental indirect band gaps for orthorhombic and tetragonal KDPs are 2.83 and 4.35 eV, respectively, by GGA. The evaluated electron effective mass in this compound is comparable to the effective mass of carrier in bilayer graphene. The electron density plots in [0 0 1] direction show strong covalent bonding within the PO_4 tetrahedra, which is symmetric in tetragonal KDP, and the symmetry is disturbed in orthorhombic KDP, where for some bonds covalency increases whereas for other decreases, due to the presence of the hydrogen bonding. The calculations of the optical spectra in the energy range 0–40 eV show that in low energies, the electronic transition occurs between O-p (valence band state) and P-p (conduction band state) for orthorhombic and tetragonal phases, whereas higher energy is related to K-p and O-s states. The evaluated dispersion results by mBJ-GGA are in better agreement with the experimental results as compared to the GGA results.

Acknowledgments

Prof. P. Blaha, Vienna University of Technology, Austria, is acknowledged for his technical help in the use of Wien2k package.

Keywords: KH_2PO_4 · optoelectronic · DFT · GGA · mBJ-GGA

How to cite this article: H. A. R. Aliabad, M. Fathabadi, I. Ahmad, *Int. J. Quantum Chem.* **2013,** *113*, 865–872. DOI: 10.1002/qua.24258

[1] C. S. Liu, C. J. Hou, N. Kioussis, S. G. Demos, H. B. Radousky, *Phys. Rev. B* **2005**, *72,* 134110.
[2] W. Lee Smith, *Appl. Opt.* **1977**, *16,* 1798.
[3] D. Xue, S. Zhang, *J. Phys. Chem. Solids* **1996**, *57,* 1321.
[4] A. Otani, S. Makishima, *J. Phys. Soc. Jpn.* **1969**, *26,* 85.
[5] A. Ioanid, M. Popescu, N. Vlahovici, I. Bunget, *Phys. Status Solidi (a)* **1984**, *82,* 125.
[6] G. Busch, *Ferroelectrics* **1987**, *72,* 1.
[7] M. E. Lines, A. M. Glass, In The International Series of Monographs on Physics, Clarendon Press: Oxford, **1977**.
[8] E. Ortiz, R. A. Vargas, B. E. Mellander, *Solid State Ionics* **1999**, *125* 177.
[9] C. Falah, L. Smiri-Dogguy, A. Driss, T. Jouini, *J. Solid State Chem.* **1998**, *141,* 486.
[10] P. Shenoy, K. V. Bangera, G. K. Shivakumar, *Cryst. Res. Technol.* **2010**, *45,* 825.
[11] G. Duchateau, G. Geoffroy, A. Dyan, H. Piombini, S. Guizard, *Phys. Rev. B* **2011**, *83,* 075114.
[12] W. R. Cook, *J. Appl. Phys.* **1967**, *38,* 1637.
[13] R. J. Nelmes, Z. Tun, W. F. Kuhs, *Ferroelectrics* **1987**, *71,* 125.
[14] P. Blaha, K. Schwarz, G. K. H. Madsen, D. Kvasnicka, J. Luitz, Wien2k, An Augmented Plane Wave plus Local orbital Program for Calculating the Crystal Properties; Techn. Uni. Wien: Austria, **2001**, ISBN3-9501031-1-2.
[15] F. Tran, P. Blaha, *Phys. Rev. Lett.* **2009**, *102,* 226401.
[16] S. Koval, J. Kohanoff, J. Lasave, G. Colizzi, R. L. Migoni, *Phys. Rev. B* **2005**, *71,* 184102.
[17] D.-F. Xue, D.-L. Xu, X. Ren, Molecular structure and nonlinear optical properties of KH_2PO_4 and $NH_4H_2PO_4$ crystals: the role of hydrogen bonds, The Proceedings of the 3rd International Conference on Functional Molecules, **2005,** 325–328.
[18] C. W. Carr, H. B. Radousky, S.G. Demos, *Phys. Rev. Lett.* **2003**, *91,* 127402.
[19] S. Koval, J. Kohanoff, R. L. Migoni, A. Bussmann-Holder, *Comput. Mater. Sci.* **2001**, *22,* 87.
[20] T. Hofmann, M. Schubert, G. Leibiger, V. Gottschalch, *Appl. Phys. Lett.* **2007**, *90,* 182110.
[21] S. Cho, M. Fuhrer, *Nano Res.* **2011**, *4,* 385–392.
[22] G. J. Snyder, E. S. Toberer, *Nat. Mater.* **2008**, *7,* 105.
[23] Z. Lin, Z. Wang, C. Chen, *J. Chem. Phys.* **2003**, *118,* 2349.
[24] V. G. Dimitriev, G. G. Gurzaddyanand D. N. Nikogosyan, Handbook of Nonlinear Optical Crystals, 2nd revised ed.; Springer: Berlin, **1977**.
[25] C. Ambrosch-Draxl, J. O. Sofo, *Comput. Phys. Commun.* **2006**, *175,* 1.
[26] S. Loughin, R. H. French, L. K. Noyer, W. Y. Ching, Y. N. Xu, *Appl. Phys.* **1996**, *29,* 1740.
[27] F. Wooten, Optical Properties of Solids; Academic Press: New York, **1972**.
[28] F. Zernike, J. E. Midwinter, Applied Nonlinear Optics; John Wiley and Sons: New York, **1973**.

Received: 20 December 2011
Revised: 2 May 2012
Accepted: 31 May 2012
Published online on 26 June 2012